JOURNAL OF GEOPHYSICAL RESEARCH, VOL. 102, NO. C6, PAGES 12,677–12,688, JUNE 15, 1997

Deterministic decomposition of deep water short-crested irregular gravity waves

Igor Prislin and Jun Zhang
Ocean Engineering Program, Department of Civil Engineering, Texas A&M University, College Station

Richard J. Seymour
Offshore Technology Research Center, College Station, Texas

Abstract. A method is developed for the deterministic decomposition of nonlinear short-crested irregular ocean waves accurate up to second order in wave steepness. Initially, an alternative maximum likelihood method is used to determine the directional spreading of wave energy. Then a least squares fitting scheme is used to calculate the initial phases of directional free-wave components. The effects of nonlinear wave-wave interactions among these free-wave components are calculated using a conventional second-order wave-wave interaction model and subtracted from the measurements. The final results are obtained through an iterative process of computing the free-wave components and their nonlinear interactions. Given an ocean wave field defined by multiple fixed-point measurements, the method is capable of decomposing the wave field into a set of directional free-wave components. On the basis of the derived free-wave components, the wave characteristics of the wave field can be predicted in the vicinity of the measurements. The method has been applied to two sets of ocean wave pressure measurements which were collected from an array of sensors mounted on an offshore production platform near the California coast. Satisfactory agreement between the predictions based on the decomposed free-wave components and related measurements indicates the proposed method is reliable. It is expected that this method will have a variety of applications to ocean science and engineering.

1. Introduction

The complex structures of short-crested irregular ocean surface waves have attracted attention from scientists and engineers for a long time. Because of this complicated physical nature of ocean waves, unidirectional and linear wave assumptions are commonly made to simplify wave modeling. As a part of the linear statistical wave assumption, random initial phases, uniformly distributed in the interval $(0, 2\pi)$ radians, are also typically assumed. Ocean waves, however, are neither unidirectional nor linear and the phases of their components may not be truly random and uniformly distributed. *Forristall et al.* [1978] showed that linear wave theory with directional spreading of wave energy predicts storm wave kinematics of the subsurface flow better than higher-order unidirectional wave theories. Nevertheless, the nonlinear wave effects are significant in predicting wave kinematics near wave crests and above mean water level [*Forristall*, 1981]. Using spectral analysis methods, the directional spectrum of a multidirectional sea can be obtained from appropriate data sets. However, no information on the initial phases of wave components is obtained. Thus the resultant wave characteristics of the measured sea, such as its wave elevation, kinematics, and pressure as a function of space and time, cannot be recovered based solely on the wave energy or amplitude spectrum. The capability of predicting wave characteristics at other than the measurement point is important to a variety of ocean science and engineering applications. Therefore it is desirable to develop a deterministic wave model allowing for both wave directionality and nonlinearity to predict ocean wave characteristics.

Short-crested irregular ocean surface waves are intuitively modeled by the superposition of free-wave components with different frequencies and propagating in different directions. The interaction among these free-wave components may change their characteristics (amplitude, frequency, wavelength, and propagating direction), and the changes are usually described as bound waves in conventional perturbation methods [*Donelan et al.*, 1985; *Zhang et al.*, 1993]. To predict the resultant wave characteristics, the decomposition of an irregular wave field into its free-wave components is necessary. While the bound wave components can be calculated straightforwardly if the free-wave components are known, conversely, the decomposition of given resultant wave measurements into its free-wave components is much more complicated because the measurements record the resultant properties of the free-wave and bound-wave components. In spite of significant progress in surface gravity wave mechanics, little has been done in decomposing directional ocean waves. The majority of attempts have been made based on linear statistical wave theory. For more references, readers are referred to *Borgman* [1990]. Attempts at deterministic decomposition of multidirectional seas using linear wave assumption are rare; see *Sand* [1979] and *Schäffer and Hyllested* [1994]. Shortcomings of these methods which consider two free-wave components at each frequency are the phase-locked decomposed wave components in Sand's method and a significant loss of energy in the decomposition (about 7–10% of total wave energy) in Schäffer

Paper number 97JC00791.
0148-0227/97/97JC-00791$09.00

and Hyllested's method. These losses could increase with steeper waves. *Masuda et al.* [1979] and *Mitsuyasu et al.* [1979] carried out a stochastic decomposition to subtract the bound-wave energy from a wind-wave energy spectrum and found that high-frequency wave components in a wind-wave field still roughly obey the linear dispersion relation. More recently, a deterministic wave model accurate up to second order in wave steepness for decomposing a unidirectional irregular wave field and predicting wave characteristics was developed by *Zhang et al.* [1996a] and validated by laboratory measurements [*Spell et al.*, 1996].

The present study intends to develop a deterministic approach for decomposing a short-crested irregular wave field into a relevant ensemble of free-wave components. On the basis of these free-wave components, the resultant wave characteristics of the wave field can be predicted. In an irregular wave field consisting of many wave components, the strongest interactions among wave components are of second order in wave steepness. Only two free-wave components are involved in each interaction. Hence the second-order wave-wave interactions between multiple free-wave components can be analytically described by the solution for the interaction between two directional monochromatic wave trains. The solution for two interacting wave trains up to the second order in wave steepness was derived using a conventional perturbation approach by *Longuet-Higgins* [1962] in deep water. Longuet-Higgins' solution is extended here for the computation of wave-induced pressure up to second order in wave steepness for multidirectional seas. It is known that when the wavelength ratio of the two wave trains is comparable to the steepness of the longer wavelength wave train, the conventional solution truncated at the second order in wave steepness may not converge. The use of the phase modulation approach can avoid this convergence difficulty [*Zhang et al.*, 1993]. Because the pressure measurements in this study were recorded by sensors located 16 m below the free surface and wave-induced pressures decay exponentially with increasing water depth, the ratios of signal to noise level for relatively high-frequency wave components were low. Consequently, the measurements were cut off above a frequency of 0.185 Hz. Therefore the convergence difficulty resulting from the interactions between wave components with disparate frequencies was not substantial, which allows us to use solely the conventional perturbation approach in the wave modeling for simplification. However, in future studies the phase modulation approach will be incorporated in the model in anticipation of the measurements of surface elevation and particle velocity near the free surface which involve strong signals at relatively high frequency.

Wave-wave interactions can be classified into "strong" and "weak" wave interactions. Strong wave interactions are observable almost immediately after waves interact, while weak wave interactions may be substantial only after hundreds of dominant wave periods [*Phillips*, 1979; *Su and Green*, 1981]. In this study, only second-order wave-wave interactions in multidirectional seas are considered, which are strong wave interactions and probably have the most relevant nonlinear effects on wave kinematics, pressures, and surface elevation within a short range from the measurements (typically a few wavelengths of the dominant wave components). Since higher-order wave interactions were ignored, the present method is not valid for the study of long-term or long-distance wave evolution, such as wave energy transfer among wave components with different frequencies [*Hasselmann*, 1962]. For decomposing a directional ocean wave field, initially, an alternative version of the maximum likelihood method (MLM) is employed to obtain a directional spectrum based on multiple fixed-point measurements [*Davis and Regier*, 1977]. This alternative MLM is briefly described in the next section. The solution for dynamic pressure induced by directional wave-wave interaction is given in section 3. The procedures for deterministic decomposition of directional sea are detailed in section 4. Field measurements from Texaco's Harvest Platform near the California coast were used for demonstrating this method. The related results are shown in section 5. The applications of this method to ocean science and engineering are introduced in section 6. Finally, the conclusions of the present study are stated and future research is discussed.

2. Directional Spectrum

Wave directionality is a crucial property of short-crested ocean waves. There are many different methods for resolving the wave directionality. Since the initial multidirectional measurements and analysis in the 1950s [*Chase et al.*, 1957], no universally accepted method for the measurements and analysis of multidirectional seas has been developed [*van Heteren et al.*, 1988; *Goda*, 1994]. A historical review of the methods was given by *Panicker* [1974] and the updates were given by *Brissette and Tsanis* [1994], and *Goda* [1994]. A wavenumber-frequency spectrum defined as $S(\mathbf{k}, f)$, relates wavenumber, frequency, and direction of wave propagation. This is known as a three-dimensional Fourier spectrum or a conditional spectrum [*Irani et al.*, 1986]. If the dispersion relation is invoked, a wavenumber-frequency spectrum reduces to a directional spectrum, or two-dimensional Fourier spectrum, which describes wave energy distribution as a function of wave propagation direction and frequency. In this study a directional spectrum based on the linear dispersion relation in deep water was obtained using the data adaptive spectral estimator (DASE), developed by *Davis and Regier* [1977], which is an alternative version of the maximum likelihood method given by *Capon* [1969].

Capon's MLM method arose from seismic data analysis methods for locating the epicenter by filtering the sharp spectral component of an earthquake process from a noisy background. It is designed to change a wavenumber window in such a way that a strong signal can be passed and other signals of different wavenumbers are suppressed. In ocean waves, not only the dominant spectral component is important but also other spectral components whose magnitudes may be relatively small, nevertheless, are still important to wave characteristics. Furthermore, there is a possibility that more than one strong spectral component exists at the same frequency but propagates in different directions. A directional spectrum derived using the original MLM algorithm may differ in wave energy from the related observed cross spectrum. This inconsistency was resolved by *Davis and Regier* [1977]. Considering the major difference between seismic and ocean wave data, they introduced an average value of the constraint that is equal to one (unit gain) over an interval around the direction of interest. They called the method as the data adaptive spectral estimator to distinguish from the MLM. Therefore, in using the DASE to derive a directional wave spectrum, there is an adjustable angular parameter that determines the size of the area in the wavenumber space. In the limit when the parameter equals to zero, the DASE is equivalent to the MLM. Numerical investigation reveals that for a small parameter, the estimated di-

rectional spectrum is larger than its true value, while for the parameter equal to 2π, the estimated spectrum is less than its true value. Therefore, there possibly exists an optimal value for the parameter; that is, when the optimal value is reached, the estimated spectrum is equal to the true value. To obtain the optimal parameter, iterative computation is used. Using the bisection method combined with the Neville cubic interpolation and the Romberg integration [*Press et al.*, 1992], the computation converges in one to two iterations and can be implemented on a personal computer.

3. Solution for Nonlinear Directional Wave-Wave Interaction

3.1. Solution for Dual Directional Waves

The solution for the interaction of dual directional gravity wave components in deep water up to the second order in wave steepness was given by *Longuet-Higgins* [1962]. The first-order solution is simply the superposition of the linear solutions for wave components 1 and 2.

$$\phi^{(1)} = \sum_{j=1}^{2} A_j e^{|\mathbf{k}_j|z} \sin \theta_j, \tag{1}$$

$$\eta^{(1)} = \sum_{j=1}^{2} a_j \cos \theta_j, \tag{2}$$

$$\theta_j = k_j \cos \beta_j x + k_j \sin \beta_j y - \omega_j t + \varepsilon_j \qquad j = 1 \text{ or } 2, \tag{3}$$

where ϕ is the potential; η is the wave elevation; θ is the linear phase; the superscript (1) denotes the first order; subscripts "1" and "2" denote the first and second wave components, respectively; t denotes time; x, y, and z are the Cartesian coordinates; z is positive upward; $z = 0$ locates at the still water level; β_j is the angle between x axis and the direction of wave component j; and ω_j, $\mathbf{k}_j$, a_j, and A_j are wave frequency, wavenumber, wave amplitude, and potential amplitude, respectively.

The dispersion relationship for deep water is

$$|\mathbf{k}_j| = \frac{\omega_j^2}{g} \qquad j = 1 \text{ or } 2, \tag{4}$$

where g is the gravitational acceleration.

The relationship between potential amplitude and elevation amplitude is given by

$$A_j = \frac{g a_j}{\omega_j} \qquad j = 1 \text{ or } 2. \tag{5}$$

Without loss of generality it is assumed that $\omega_1 \geq \omega_2$.

The second-order solution for velocity potential and elevation is given by

$$\phi^{(2)} = \phi_-^{(2)} + \phi_+^{(2)}, \tag{6}$$

$$\phi_\mp^{(2)} = A_1 A_2 k_1 k_2 B_0^{\mp}(\omega_1 \mp \omega_2) \cdot [\cos(\beta_1 - \beta_2) \pm 1] e^{|\mathbf{k}_1 \mp \mathbf{k}_2|z} \sin(\theta_1 \mp \theta_2), \tag{7}$$

$$\eta^{(2)} = \eta_-^{(2)} + \eta_+^{(2)} + \sum_{j=1}^{2} \eta_j^{(2)}, \tag{8}$$

$$\eta_j^{(2)} = \tfrac{1}{2} a_j^2 k_j \cos 2\theta_j \qquad j = 1 \text{ or } 2, \tag{9}$$

$$\eta_\mp^{(2)} = a_1 a_2 \cos(\theta_1 \mp \theta_2) \left\{ \sqrt{k_1 k_2}\,[\cos(\beta_1 - \beta_2) \pm 1] \cdot \left[B_0^{\mp}(\omega_1 \mp \omega_2)^2 - \frac{1}{2} \right] + \frac{k_1 + k_2}{2} \right\}, \tag{10}$$

$$B_0^{\pm} = \frac{1}{(\omega_1 \pm \omega_2)^2 - g|\mathbf{k}_1 \pm \mathbf{k}_2|}. \tag{11}$$

where superscript "(2)" denotes the second order and the subscripts "−" and "+" denote the difference and sum interactions between the components, respectively.

On the basis of the solution for the potential, wave characteristics such as pressure, particle velocity, and particle acceleration can be computed up to second order in wave steepness. In our case the pressure head measurements are used in the decomposition. The equation for the pressure head at a fixed point is derived below. The equations for horizontal velocity components are given in the Appendix. Substituting linear and second-order solutions into the Bernoulli equation, the total pressure head at $z = -d$ up to second order in wave steepness is given by

$$p = p^{(1)} + p_-^{(2)} + p_+^{(2)} + \bar{p}, \tag{12}$$

where the pressure components are given in the following equations.

Linear pressure head is given by

$$\frac{p^{(1)}}{\rho g} = \sum_{j=1}^{2} a_j e^{-k_j d} \cos \theta_j. \tag{13}$$

Pressure heads related to wave-wave difference and sum interactions are given by

$$\frac{p_\mp^{(2)}}{\rho g} = a_1 a_2 \sqrt{k_1 k_2}\,[\cos(\beta_1 - \beta_2) \pm 1] \cos(\theta_1 \mp \theta_2) \times \left[B_0^{\mp}(\omega_1 \mp \omega_2)^2 e^{-|\mathbf{k}_1 \mp \mathbf{k}_2|d} - \frac{1}{2} e^{-(k_1 + k_2)d} \right], \tag{14}$$

The static pressure head due to hydrostatic pressure and second-order wave interactions is given by

$$\frac{\bar{p}}{\rho g} = d - \frac{1}{2} \sum_{j=1}^{2} a_j^2 k_j e^{-2k_j d}. \tag{15}$$

It is noted that the second harmonic of the pressure head is not present because the second harmonic of the velocity potential is equal to zero and no contribution is made from the squared velocity term in deep water. Equations (12)–(15) are crucial for the nonlinear wave decomposition. The constant terms shown in (15) are subtracted from the measurements first. In the Fourier analysis they correspond to the zero frequency coefficient.

3.2. Solutions for Multiple Wave Components

The first-order pressure at jth sensor is simply the superposition of the pressures induced by all free-wave components,

$$\frac{p^{(1)}}{\rho g} = \sum_{n=1}^{N} \sum_{m=1}^{M} a_{mn} e^{-k_{mn} d} \cos(\theta_{mn}), \tag{16}$$

$$\theta_{mn} = \mathbf{k}_{mn} \cdot \mathbf{x}_j - \omega_n t + \varepsilon_{mn}, \tag{17}$$

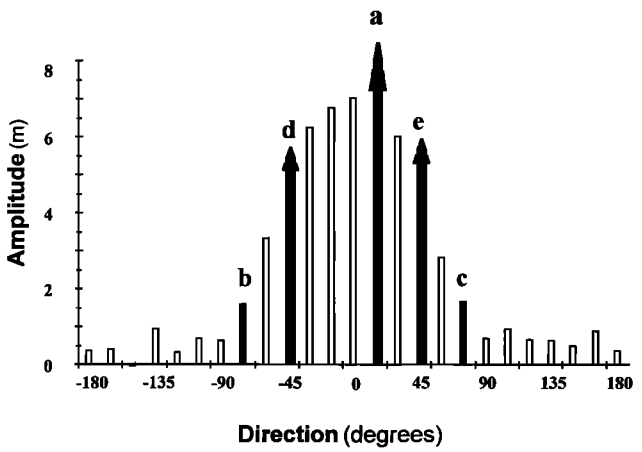

Figure 1. Directional spreading and reduced number of free-wave components per frequency.

where M is the number of free-wave components at each frequency, N is the number of discretized frequencies, a_{mn} is the amplitude of a free-wave component, $\mathbf{k}_{mn}$ is the wave number, ω_n is the wave frequency, and ε_{mn} is the initial phase. The horizontal coordinate vector of the jth sensor is $\mathbf{x}_j$.

Since only two free-wave components are involved in each second-order wave-wave interaction, the solution for second-order pressure head in a multidirectional wave field can be extended according to (14). The solutions for difference and sum types second-order pressures are given by

$$\frac{p_{\mp}^{(2)}}{\rho g} = \sum_{n_1=n_2+1}^{N} \sum_{m_1=1}^{M} \sum_{n_2=1}^{N-1} \sum_{m_2=1}^{M} a_{m_1n_1} a_{m_2n_2} \sqrt{k_{m_1n_1} k_{m_2n_2}} \left\{ \{B_0^{\mp}(\omega_{n_1} \mp \omega_{n_2})^2 \cdot \exp\left(-|\mathbf{k}_{m_1n_1} \mp \mathbf{k}_{m_2n_2}|d\right) - \frac{1}{2}\exp\left[-(k_{m_1n_1} + k_{m_2n_2})d\right] \right\} \cdot [1 \pm \cos(\beta_{m_1n_1} - \beta_{m_2n_2})] \cos(\theta_{m_1n_1} \mp \theta_{m_2n_2}), \quad (18)$$

$$B_0^{\pm} = \frac{1}{(\omega_{n_1} \pm \omega_{n_2})^2 - g|\mathbf{k}_{m_1n_1} \pm \mathbf{k}_{m_2n_2}|}. \quad (19)$$

where the index m stands for the direction and n stands for the frequency.

4. Procedures for Deterministic Decomposition of Directional Seas

To achieve relatively fine resolution in determining wave energy directional spreading based on a few simultaneous wave records, the decomposition of a directional irregular wave field starts with the use of the DASE described in section 2. Since the DASE does not retain the complete information of wave components, the initial phases of free-wave components are recovered using a fitting procedure of prediction with input data. Then the effects due to the nonlinear interaction among free-wave (linear) components are computed and subtracted from the resultant wave properties, i.e., measurements. At the first iteration the measurements are used as input data. After that the input data will be the measurements subtracting the nonlinear wave effects. Thus the new input data can be viewed as the summation of the free-wave components. These three major steps in the decomposition, wave direction estimation, initial phase computation, and the decoupling of the effects of nonlinear wave interactions, are detailed below.

4.1. Estimation of Wave Direction and Selection of Directional Free-Wave Components

In using the DASE, directional resolution is set to 4°, which gives 90 directional wave components at each frequency. The number of discrete frequencies is determined by the length of the time series as well as the cutoff frequency. To reduce the computation time, only a finite number (say 1, 3, or 5) of directional free-wave components at each frequency are used to approximate the energy spreading. The selection of how many free-wave components at each frequency and then their respective directions and amplitudes are based on the wave directional spreading obtained using the DASE. The following description is based on a unimodal direction spreading, which is relevant to the ocean waves studied in section 5.

Given the directional energy spreading, the component with the largest amplitude at each frequency, named as the most energetic component, can be identified, and its propagation direction, denoted as β_0, is considered as the main direction of wave propagation at this frequency. In anticipation of asymmetric directional spreading with respect to the main propagation direction, the normalized left- and right-hand side first Π_1 and second Π_2 moments with respect to the most energetic component at this frequency are computed. For simplicity, only the definitions of the left-hand side moments are given below.

$$\Pi_1 = \frac{\int_{\beta_0-\pi}^{\beta_0} (\beta - \beta_0)a^2\, d\beta}{\int_{\beta_0-\pi}^{\beta_0} a^2\, d\beta} \quad (20)$$

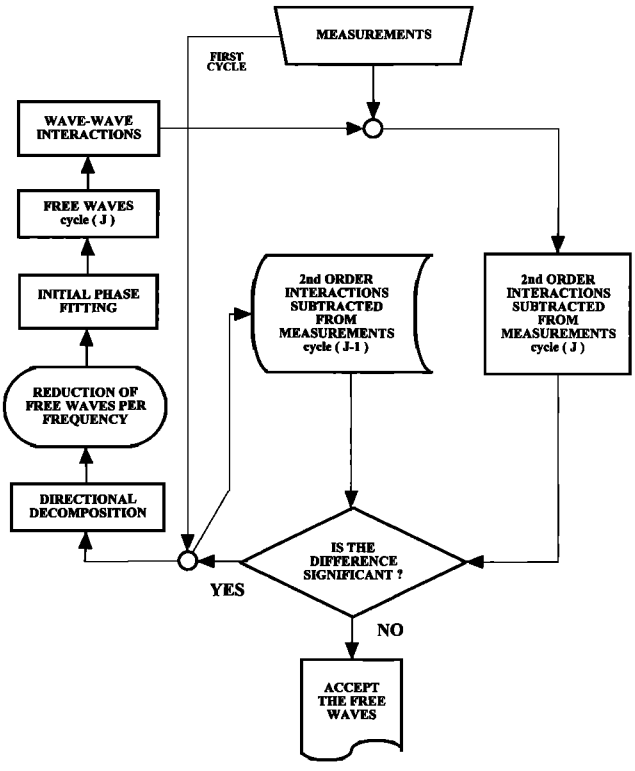

Figure 2. Flowchart for wave decomposition.

$$\Pi_2 = \frac{\int_{\beta_0-\pi}^{\beta_0} (\beta - \beta_0)^2 a^2 \, d\beta}{\int_{\beta_0-\pi}^{\beta_0} a^2 \, d\beta} \tag{21}$$

where β and a^2 are the direction angle and amplitude square of free-wave components. The magnitude of these moments may indicate the extent of directional spreading at each frequency. Smaller magnitudes of moments are corresponding to narrow directional spreading, while greater ones are corresponding to wide directional spreading. If only a single (Dirac) free-wave components exists at this frequency, the moments are equal to zero. The opposite extreme case (not likely in nature) is wave energy evenly distributed from 0 to 2π. Its first and second moments are $\pi/2$ and $\pi^2/3$, respectively. In terms of the commonly used energy spreading function $\cos^{2s}[(\beta - \beta_0)/2]$, where s is a measure for the narrowness of the energy spreading and is assumed to be around 10 for wind waves and 50 for swells [*Goda*, 1981], the first and second moments are 0.35 and 0.19 for $s = 10$ and 0.16 and 0.04 for $s = 50$, respectively. It is found that for our case 1 the first moments for the left and right parts of the spectral spreading for dominant frequency are around -0.22 and 0.23, respectively. The second moments are 0.09 and 0.11, respectively. For our case 2 the first moments are -0.09 and 0.20, respectively, and the second moments are 0.01 and 0.33, respectively. Relatively large moments for the right part of the spectral spreading in case 2 result from the presence of different direction swell and wind waves. The number of free-wave components at each frequency is determined according to the magnitude of the first and second moments. If the magnitudes of the moments are small, one free-wave component at each frequency seems to be sufficient. With the increase in their magnitudes, more free-wave components at each frequency are used to describe the energy spreading. In our computation, always equal numbers of free-wave components are located at both sides of the most energetic wave component. The direction of the most left-side free-wave component is determined by the ratio of moments.

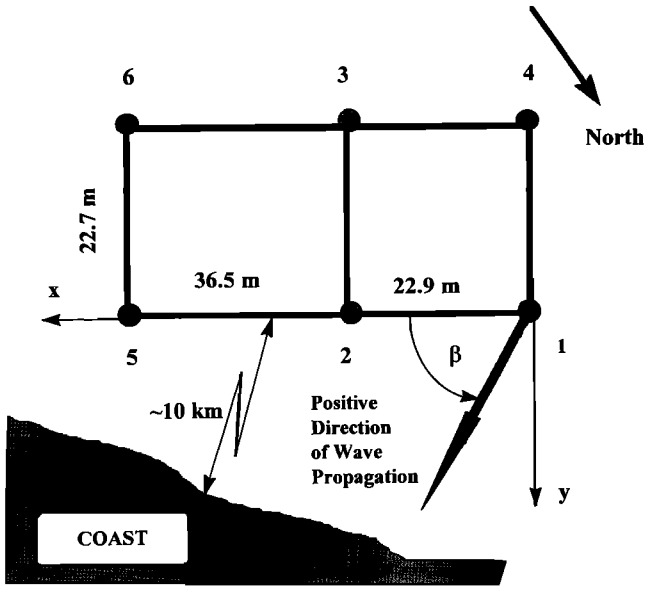

Figure 3. Pressure-sensor array at Harvest Platform.

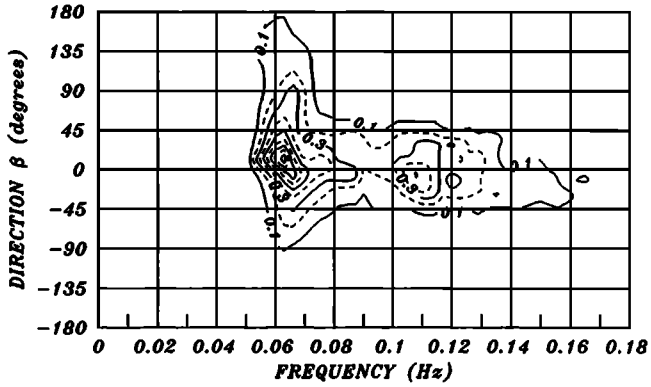

Figure 4. Normalized directional pressure amplitude spectrum in the range from 0.1 to 1.0 of the spectral peak for case 1.

$$\beta_l = \frac{\Pi_2}{\Pi_1} \tag{22}$$

If more than one free-wave components is used at the left-hand side of the most energetic components, then the directions of remaining left-side free-wave components are evenly distributed between the most left-side free-wave components and the most energetic components as sketched in Figure 1. In numerical computation the above determined directional angles are rounded to the nearest discrete angles used in the DASE. The selection of free-wave components at the right-hand side of the most energetic component is virtually the same as those at the left-hand side.

After the number of the free-wave components and their directions at each frequency are determined, their amplitudes can be determined according to the following two equations:

$$B_m = \mu A_i, \quad \text{for} \quad \beta_m = \beta_i \tag{23}$$

where A_i is the amplitude of the ith components among M_0 wave components obtained using the DASE and B_m is the amplitude of the mth wave components of M selected components (usually $M \ll M_0$). The scaling factor μ is larger than unity and given by

$$\mu = \sqrt{\frac{\sum_{i=1}^{M_0} A_i^2}{\sum_{m=1}^{M} B_{om}^2}} \tag{24}$$

B_{om} is virtually a subset of A_i and is defined by $B_{om} = A_i$ for $\beta_m = \beta_i$ and $B_{om} = 0$ for $\beta_m \neq \beta_i$. Equation (24) ensures that the total energy of the finite free-wave components is equal to that obtained from the DASE, while (23) ensures that the energy spreading of the M components as a function of β approximately resembles that of M_0 components obtained using the DASE. It should be noted that the above selection procedures are reliable in our computation but may not be optimal. In the future, more data of ocean waves are needed to verify and improve them.

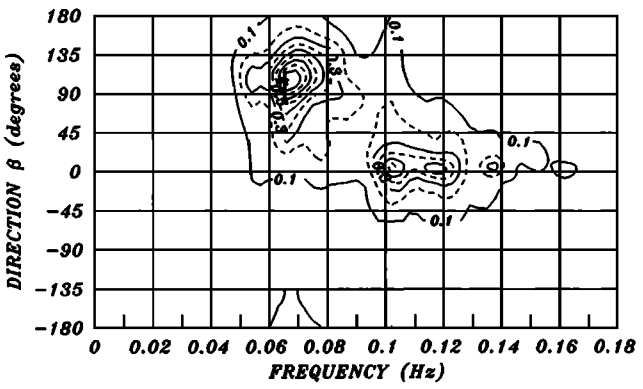

Figure 5. Normalized directional pressure amplitude spectrum in the range from 0.1 to 1.0 of the spectral peak for case 2.

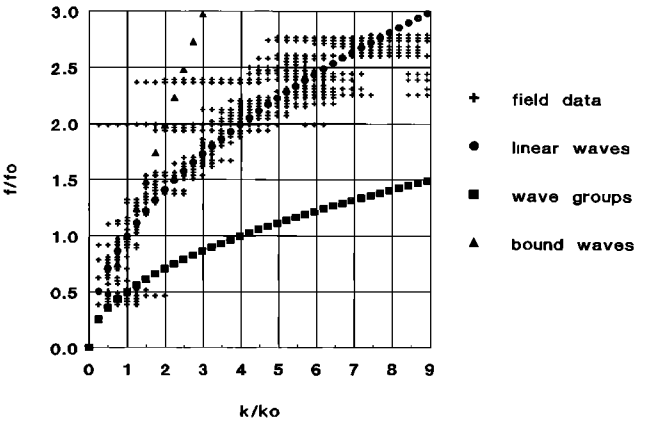

Figure 6. Conditional wavenumber-frequency spectrum for case 2.

4.2. Determining Initial Phases and Decoupling Nonlinear Effects From Measurements

The initial phases of the free-wave components can be solved from the following equation:

$$\sum_{m=1}^{M} a_{mn} e^{-k_{mn}d} \cos(\mathbf{k}_{mn}\mathbf{x}_j + \varepsilon_{mn}) = \frac{P_{jn}}{\rho g} \cos(\varphi_{jn}) - \mathcal{E}_{jn} \qquad (25)$$

$$j = 1, \cdots, J \qquad n = 1, \cdots, N$$

where P_{jn} and φ_{jn} are the modulus and phase of the Fourier coefficients of the measured pressure and $\mathcal{E}_{jn}$ is the pressure head induced by nonlinear interaction among free-wave components at the nth frequency and at the jth sensor, defined as

$$\mathcal{E}_{jn} = \frac{p_-^{(2)}}{\rho g} + \frac{p_+^{(2)}}{\rho g}. \qquad (26)$$

Equation (25) requires that at the jth sensor the sum of the pressure of free-wave components at frequency n be equal to the measured pressure subtracting the nonlinear pressure at the same frequency. In this study, only second-order nonlinear effects are considered in (26), and its computation was detailed in section 3.2 and hence is not repeated here. Equation (25) is solved in the frequency domain. For simplicity the subscript n denoting the frequency will be dropped in later description. At each frequency, there are $2J$ real equations and M unknowns (ε_m). Allowing the decomposition to use any number of measurements J, but not less than three, we do not rigidly request $J = M/2$. Therefore the number of equations and unknowns may not be the same. In addition, (25) is not linear because of the constraint $\sin^2(\varepsilon_m) + \cos^2(\varepsilon_m) = 1$. For these two reasons we do not attempt to solve (25) for exact solution but instead for an approximate solution using the least squares approach whose algorithm is outlined below.

The approximate solution for the initial phases at each frequency is obtained through the minimizing the target function which is sum of error squares.

$$\Re = \sum_{j=1}^{J} |\Delta_j|^2 \Rightarrow \min. \qquad (27)$$

where Δ_j is complex and denotes the differences between the two sides of (25) at the jth sensor. The exact solution of (25) is corresponding to a zero target function. The minimum of the target function is searched by systematically varying the magnitudes of the initial phases in a multidimensional space of dimension M. The minimization of the target function is accelerated in our computation using a conjugate gradient minimization algorithm, known as the Fletcher-Reeves-Polak-Ribiere method [*Press et al.*, 1992]. The search for the approximate solution of initial phases is accomplished when the target function is smaller than a preset tolerance for errors.

After the phases, directions, and amplitudes of discretized free-wave components are initially calculated, the pressure head contributed from second-order nonlinear wave-wave interactions can be computed and subtracted from the measurements. The amplitudes, phases, and directions of the free-wave components can then be recomputed based on the new input data, that is, the measurements subtracting nonlinear contributions. This iteration will continue until the difference between the results of two consecutive iterations is smaller than a preset tolerance. The flowchart of iteration is depicted in Figure 2.

Table 1. Correlation Coefficients Between Measured and Computed Signals for Case 1

Model		Correlation Coefficient					
Free Waves per Frequency	Sensors	Sensor 1	Sensor 2	Sensor 3	Sensor 4	Sensor 5	Sensor 6
1	1, 2, 3	0.988	0.994	0.989	0.982*	0.975*	0.975*
1	1, 2, 3, 4	0.988	0.992	0.990	0.986	0.973*	0.974*
1	1, 2, 3, 4, 5	0.985	0.993	0.990	0.985	0.979	0.977*

*The coefficient belongs to predicted signal.

Table 2. Standard Errors Between Measured and Computed Signals for Case 1

Model		Sensor 1		Sensor 2		Sensor 3		Sensor 4		Sensor 5		Sensor 6	
Free Waves per Frequency	Sensors	Standard Error, m	Standard Error, %	Standard Error, m	Standard Error, %	Standard Error, m	Standard Error, %	Standard Error, m	Standard Error, %	Standard Error, m	Standard Error, %	Standard Error, m	Standard Error, %
1	1, 2, 3	0.069	5.7	0.049	4.3	0.067	5.4	0.086*	7.0*	0.096*	9.5*	0.097*	8.6*
1	1, 2, 3, 4	0.071	5.9	0.054	4.7	0.065	5.2	0.077	6.3	0.099*	9.7*	0.100*	8.9*
1	1, 2, 3, 4, 5	0.076	6.2	0.052	4.6	0.063	5.1	0.081	6.6	0.088	8.7	0.093*	8.3*

*The coefficient belongs to predicted signal.

5. Field Measurements and Numerical Results

Ocean pressure measurements are used to verify the directional wave model for decomposition. In the future we will use measurements of other wave characteristics, such as surface elevation and wave kinematics, in the decomposition. The pressure measurements were collected from an array of pressure sensors mounted on the Texaco Harvest offshore oil production platform, approximately 16 m below the sea surface (see Figure 3). The platform is a fixed structure located about 10 km west of Point Conception in a water depth of 225 m. Hence, in our computation, all wave components with significant amplitudes are considered as deep water waves. The data are transferred to the Coastal Data Information Program (CDIP) at the Scripps Institution of Oceanography at 3-hour intervals. Details of the data acquisition and analysis system are described by *Seymour et al.* [1993]. Additional information and graphical images are accessible on the internet through the URL address http://splash.ucsd.edu.

Two sets of pressure head data representing the sea states on May 7 and May 24, 1993, were selected for this study. They are referred as case 1 and case 2, respectively. Case 1 involves a swell and local wind waves both from the northwest direction (see Figure 4), whereas case 2 is the combination of a swell from the south and the local wind waves from the northwest (see Figure 5). The significant wave heights, estimated from frequency spectra, were 3.31 m and 1.29 m for case 1 and case 2, respectively. The sampling rate in both cases is 1 Hz (Nyquist frequency equals to 0.5 Hz). A time series of 512 s was selected from records exceeding 2 hours in length. We limit the duration of the time series to approximately 8.5 min, assuming that within that period of time the wave properties such as wave amplitudes and directions of propagation are approximately stationary. The shortest wavelength (the highest wavenumber) which can be resolved due to the aliasing is twice the smallest distance between sensors [*Donelan et al.*, 1985]. For the Harvest Platform array the smallest distance between sensors is 22.7 m (Nyquist wavenumber equal to 0.1384 m^{-1}). This limit should be invoked if the linear dispersion relationship is not assumed [*Donelan et al.*, 1985; *Irani et al.*, 1986]. In this study the linear dispersion relationship was imposed in the DASE to find the wave directional spreading. In our analysis we set the cutoff frequency to 0.185 Hz because the signal to noise ratio was weak above that value.

Table 3. Correlation Coefficients Between Measured and Computed Signals for Case 2

Model		Correlation Coefficient			
Free Waves per Frequency	Sensors	Sensor 1	Sensor 2	Sensor 3	Sensor 4
1	1, 2, 3	0.983	0.991	0.987	0.973*
3	1, 2, 3	0.990	0.995	0.994	0.973*
5	1, 2, 3	0.993	0.996	0.996	0.978*
7	1, 2, 3	0.995	0.996	0.997	0.978*

*The coefficient belongs to predicted signal.

There are six pressure sensors on the platform, and their positions are marked as solid circles in Figure 3. For case 1 we had measurements from all six sensors, but for case 2, only measurements from sensors 1 to 4 are available. In analyzing the data of case 1, two sets of measurements, from three sensors (1–3) and from four sensors (1–4), were used for wave decomposition. The time series from the fifth and the sixth sensors (see Figure 3) were reserved for later comparison with the predictions, and hence they were deliberately excluded from the signal decomposition. Similarly, for case 2 we used measurements from sensors 1–3 for the signal decomposition. The time series from the sensor 4 was reserved for comparison.

The directional pressure amplitude spectra shown in Figures 4 and 5 are obtained using the DASE and assuming the linear dispersion relationship in deep water. Figure 6 shows the relationship between the wavenumber and frequency of wave components for case 2. It was determined according to *Irani et al.* [1986], also based on the DASE but without invoking the linear dispersion relationship. The wave components whose energy is less than 20% of the energy of the most energetic wave component at the same frequency are not plotted. The plotted values in Figure 6 show that the wavenumber and frequency of the majority of the wave components do obey the deep water linear dispersion relationship. As expected, the nonlinear effects are mainly shown at high and low frequencies with respect to the spectral peak frequency.

Using the numerical scheme described in section 4, the short-crested irregular ocean waves are deterministically decomposed and parameters of wave components, such as amplitudes, directional angles, and initial phases at each frequency, are determined. They can be used for the prediction of resultant characteristics of the wave field. It should be noted that the total wave energy is preserved at each step in our method, in contrast to the about 7–10% of total wave energy loss in the method by *Schäffer and Hyllested* [1994] which considers two free waves per frequency.

The accuracy and feasibility of our method are examined in two different tests. The first test involves the comparison of the predicted pressure time series with the related filtered measurements used as input in the deterministic decomposition. The measured time series are filtered with a low-pass numerical filter with the cutoff frequency of 0.185 Hz. This kind of

Table 4. Standard Errors Between Measured and Computed Signals for Case 2

Model		Sensor 1		Sensor 2		Sensor 3		Sensor 4	
Free Waves per Frequency	Sensors	Standard Error, m	Standard Error, %	Standard Error, m	Standard Error, %	Standard Error, m	Standard Error, %	Standard Error, m	Standard Error, %
1	1, 2, 3	0.034	6.4	0.025	4.9	0.030	5.3	0.043*	7.8*
3	1, 2, 3	0.027	5.1	0.018	3.5	0.020	3.6	0.043*	7.8*
5	1, 2, 3	0.021	4.0	0.016	3.2	0.010	2.9	0.040*	7.2*
7	1, 2, 3	0.019	3.6	0.015	3.0	0.015	2.6	0.039*	7.2*

*The coefficient belongs to predicted signal.

predicted pressure time series is referred to a recovered signal. The test examines whether or not the iteration in our numerical scheme converges. The second test is more comprehensive and involves the comparison of the prediction with the related measurements not used as input in deterministic decomposition. This kind of prediction is referred to as a predicted signal. The test may reveal whether or not the deterministic decomposition can be realized using a limited number of directional wave components at each frequency and how the number of wave components affects the accuracy of wave predictions.

The correlation coefficients and the standard (RMS) errors between the measured and computed pressure heads are given in Tables 1–4. The standard error is the root-mean-square (RMS) error between measured and calculated signals, and it is given in meters as well as in percentages of the maximum pressure head amplitude in the time-series. In addition, the related pressure heads as a function of time are compared in Figures 7–10 for case 1 and in Figures 11–14 for case 2. As shown in Tables 1–4 and in Figures 7–14, the measured and calculated pressure heads match very well. In general, all comparisons show that the standard (RMS) error is within the range 5–7% for the recovered signals and 7–10% for the predicted signals. Occasionally, there are some small deviations from the measured pressure heads (see Figures 11 and 14 at local time around 70 s).

The effect of the number of sensors used in the wave decomposition on accuracy of the prediction has been explored. The number of sensors used in the wave decomposition varied from three to five in case 1 as indicated in Tables 1 and 2. It seems that there is not significant improvement in correlations or standard errors due to the increase in the number of sensors. We suspect that this may be caused by the redundant arrangement in the sensor array at Harvest Platform (see Figure 3). The pairs of sensors 1–2, 3–4, and 2–5 are redundant, as well as the pairs of sensors 1–4 and 2–3.

For narrow and unimodal directional wave energy spreading, as observed in cases 1 and 2, the increase in the number of wave components per frequency reduces the standard error for the recovered signals but only slightly improves the accuracy in the predicted signals. As shown in Tables 3 and 4 for case 2, the standard error is reduced by 40–50% in the recovered signals by increasing the number of wave components from one to seven per frequency. The reduction of the standard error with the increase in the number of waves per frequency is expected because more wave components provide more degrees of freedom for minimizing the target function. In contrast, the reduction of the standard error is not significant for the predicted signals. Therefore, when the directional spreading of wave energy is narrow, even when its main direction varies with different frequencies, it appears that this kind of directional wave fields can be modeled using a single wave component at each frequency, i.e., using the most energetic directional wave component at each frequency. This finding may greatly simplify the model of unimodal and narrow spreading directional wave fields. However, further investigations and experimental verifications are required.

Wave directionality is essential for the accurate computation of wave characteristics. To demonstrate that, we preserved the same energy frequency spectrum for cases 1 and 2 but assumed that all wave components were unidirectional in the direction

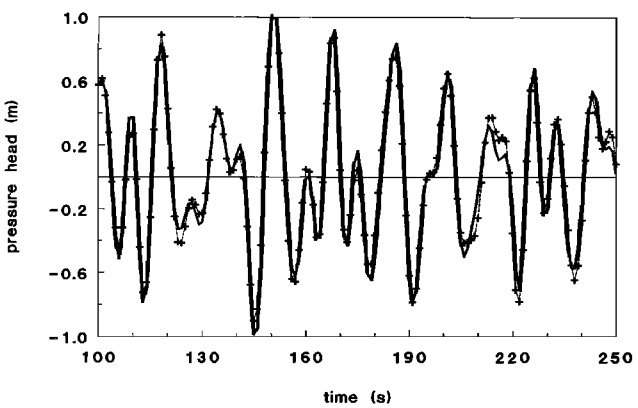

Figure 7. Recovered pressure head time series 1 for case 1; model: one wave, three sensors. Solid curve, input; solid curve with pluses, recovered.

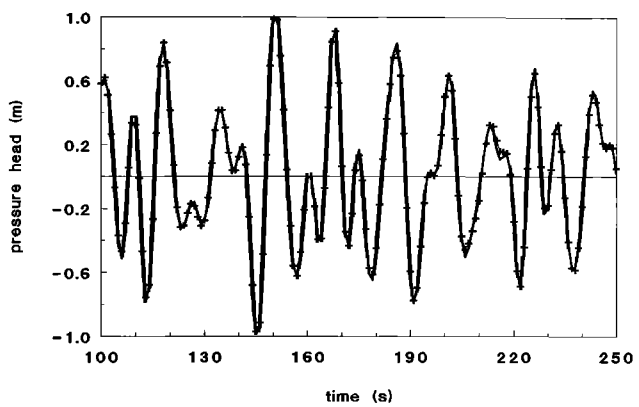

Figure 8. Recovered pressure head time series 1 for case 1; model: five waves, three sensors. Solid curve, input; solid curve with pluses, recovered.

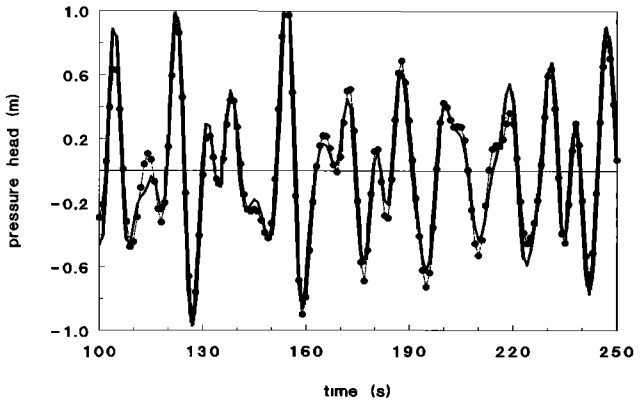

Figure 9. Predicted pressure head time series 6 for case 1; model: one wave, three sensors. Solid curve, input; dashed curve with circles, predicted.

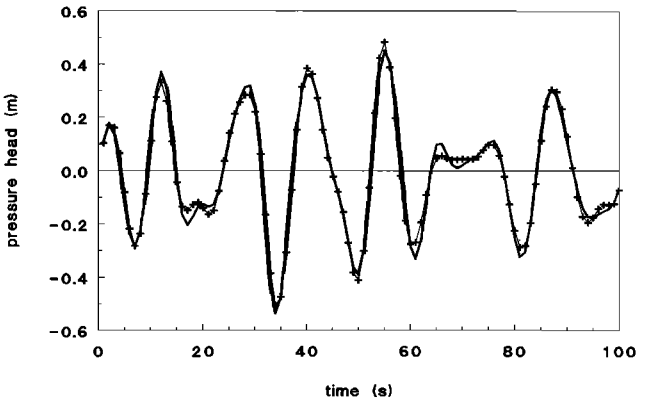

Figure 11. Recovered pressure head time series 1 for case 2; model: three waves, three sensors. Solid curve, input; solid curve with pluses, recovered.

of zero degree angle, which is the approximate dominant direction, for both swell and wind waves in case 1 and only the dominant direction for wind waves in case 2. Then we simulated time series and compared them with the filtered measured time series. The correlation coefficients are presented in Table 5. As expected, at sensor 1 the correlation coefficient is almost unity in both cases 1 and 2. This is because sensor 1 is located at the origin of the coordinates, and, consequently, the wavenumber vector (directionality) does not make a contribution to the phases of wave components. While the correlation coefficients of unidirectional waves at other sensors are only slightly inferior to those of directional waves in case 1, they become much worse in case 2. In case 1 the directions of most energetic wave components of almost all frequencies are around 0°; the approximation of unidirectional wave in that direction renders reasonable predictions, although not as well as those allowing for wave directionality. However, in case 2 the dominant direction of wind waves is still around zero, but the dominant direction of the swell is around 100°. It is not surprising to see that the assumption of unidirectional waves leads to large discrepancies between the measurements and predictions. The smallest correlation coefficient appearing at sensor 3 is 0.635, although the distance between sensors 1 and 3 is around 32 m, which is much shorter than the spectrum peak wavelength.

The assumption that the waves are unidirectional also has serious consequences in wave kinematics prediction. The particle velocities as a function of depth at the location of sensor 1 and local time 167 s are shown as lines with open symbols for multidirectional waves and lines with solid symbols for unidirectional waves in Figure 15. It shows that the corresponding velocity components generally differ and the greatest differences occur near the free surface. Another application can be related to the wave measurements. For example, the velocity in the x direction for the unidirectional wave is about 13% higher than for the multidirectional wave. In addition, the resultant horizontal velocity of a multidirectional wave field changes with water depth not only in magnitude but also in direction, which is demonstrated in Figure 16. In Figures 17, 18, and 19 the computed particle velocity components as functions of time are shown for case 2 at the location of sensor 3. The particle velocity components as functions of depth are shown in Figure 20 at local time 40 s. It is interesting to notice that the x direction velocity component reverses its direction at approximately 27 m below the surface. This trend was not observed when the unidirectional wave assumption was used.

To examine the effects of second-order wave nonlinearity on the prediction of pressure head, the pressure heads at sensor 4

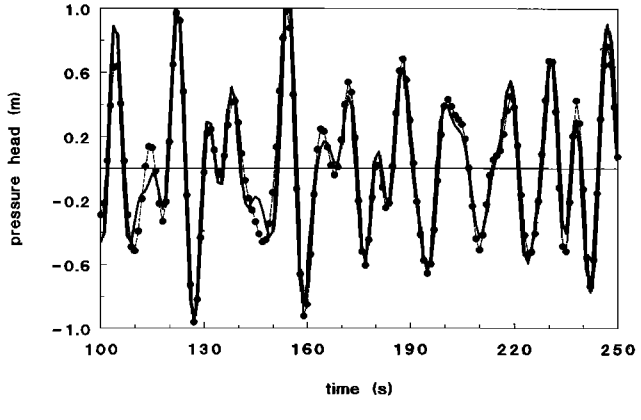

Figure 10. Predicted pressure head time series 6 for case 1; model: five waves, three sensors. Solid curve, input; dashed curve with circles, predicted.

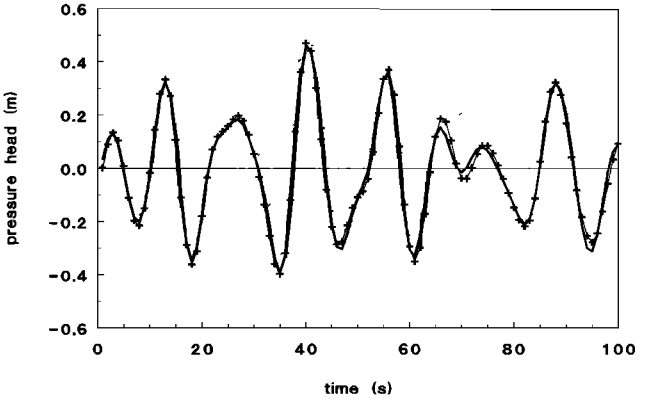

Figure 12. Recovered pressure head time series 2 for case 2; model: three waves, three sensors. Solid curve, input; solid curve with pluses, recovered.

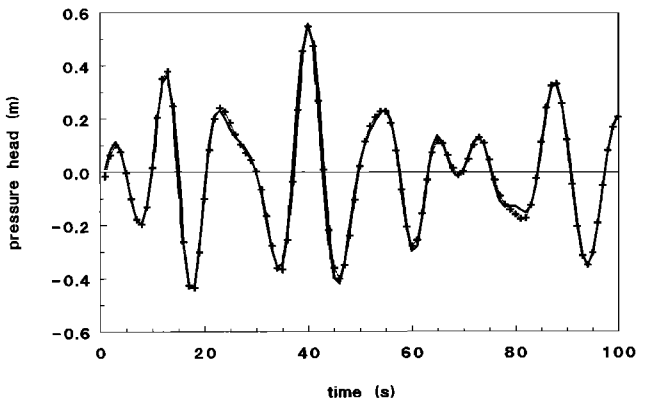

Figure 13. Recovered pressure head time series 3 for case 2; model: three waves, three sensors. Solid curve, input; solid curve with pluses, recovered.

in cases 1 and 2 were also predicted using linear wave theory based on the measured pressure heads at sensors 1–3. In using linear wave theory, the term $\mathcal{E}_{jn}$ in (25) representing the pressure head resulting from nonlinear wave-wave interaction is set to zero in the decomposition as well as prediction. The correlation between the predictions using linear wave theory and the corresponding measured pressure head at sensor 4 is 0.978 in case 1 and 0.973 in case 2. The related correlation of the predictions considering nonlinear effects is 0.982 for case 1 (see Table 1) and 0.973 for case 2 (see Table 3). The improvement due to the considering nonlinear effects on pressure heads is not significant. It is because the measured ocean waves in cases 1 and 2 were not very steep and the pressure sensors were deployed relatively far away from the free surface. As a result the nonlinear effects on the measured pressure heads in cases 1 and 2 are insignificant. However, our ongoing research on the prediction of surface elevation based on pressure head measurements indicates that the nonlinear effects may be significant, if the measured waves are very steep or pressure sensors are located relatively close to the free surface [*Zhang et al.*, 1996b]. These results will be reported in the near future.

Table 5. Correlation Coefficients Between Measured and Simulated Pressure Signal Based on Unidirectional Wave Model

	Correlation Coefficient				
Case	Sensor 1	Sensor 2	Sensor 3	Sensor 4	Sensor 5
1	0.966	0.968	0.932	0.935	0.928
2	0.988	0.856	0.635	0.921	···

6. Applications

Although it is generally acknowledged that wave energy directional spreading is an important feature of ocean waves, directional spectra for ocean waves have not been widely used in the design of offshore structures [*Sand*, 1979; *Goda*, 1994]. This is due mainly to the lack of reliable measurements of three-dimensional waves and also to insufficient theoretical supports for solving the inverse irregular wave problem, i.e., the decomposition of measured irregular waves into its linear components [*Long*, 1986]. For example, various types of instruments, such as surface piercing wave gages, pressure sensors, and velocimeters are used to measure multidirectional seas. To ensure that these measurements are accurate or that a wave model based on these measurements is capable of predicting wave characteristics accurately, it is essential to compare the prediction (say velocity) based on one type of measurements (say elevation) with the related measurements. A definite conclusion can be reached through the match of related prediction and measurement in the time domain. The method developed in this study is capable of predicting ocean wave characteristics in the vicinity of the measurements and hence may be used to compare the measurements obtained from different instruments.

Because ocean waves are neither completely linear nor unidirectional, this method based on a multidirectional nonlinear wave model certainly can provide more useful information than methods based on a unidirectional wave model. Hence the potential of applying this method to ocean science and offshore engineering is expected to be great. It is believed that directional wave loadings influence the torsion moments on a tension leg platform, the yaw motions of an offshore structure, and the accumulation of fatigue damage on steel jacked struc-

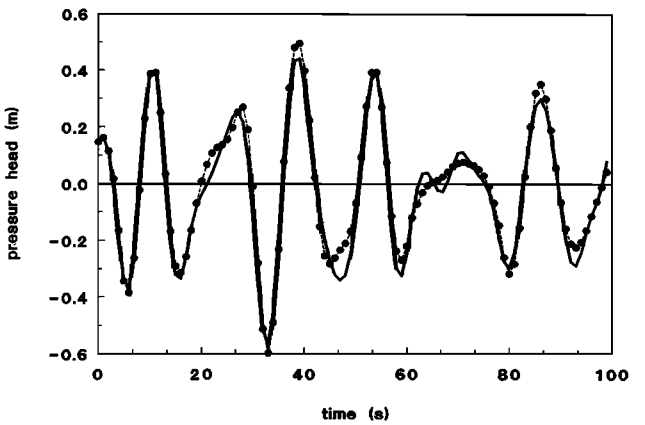

Figure 14. Predicted pressure head time series 4 for case 2; model: three waves, three sensors. Solid curve, input; dashed curve with circles, predicted.

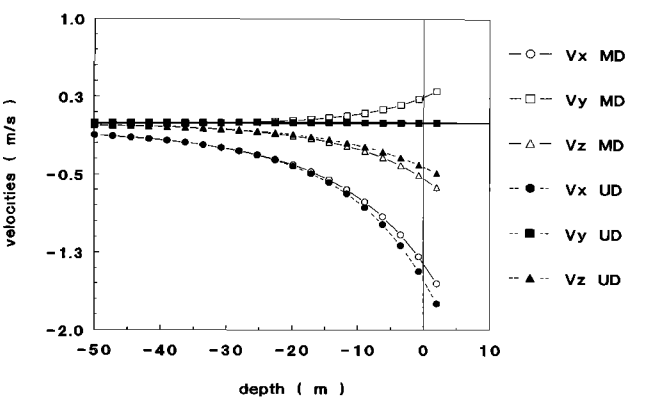

Figure 15. Particle velocities up to second order of multidirectional (MD) and unidirectional (UD) waves for case 1 (model: one wave, three sensors) at sensor location 1 and local time 167 s.

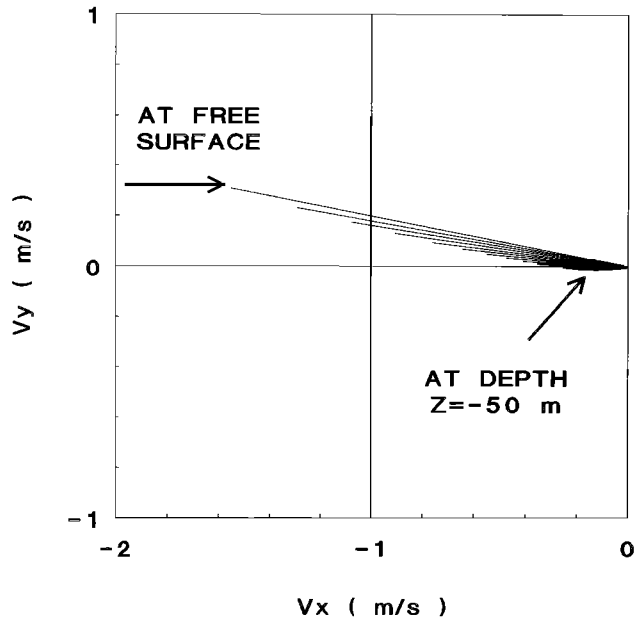

Figure 16. Horizontal velocity vector as a function of depth for case 1 (model: one wave, three sensors) at sensor location 1 and local time 167 s.

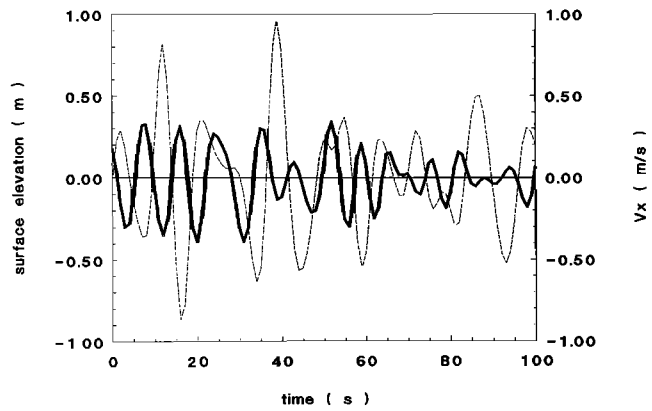

Figure 17. Predicted velocity V_x at free surface for horizontal location of sensor 3 for case 2 (model: three waves, three sensors). Dashed curve, surface elevation; solid curve, velocity.

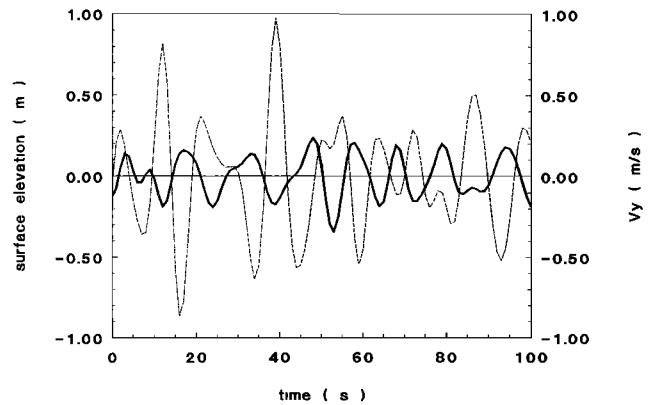

Figure 18. Predicted velocity V_y at free surface for horizontal location of sensor 3 for case 2 (model: three waves, three sensors). Dashed curve, surface elevation; solid curve, velocity.

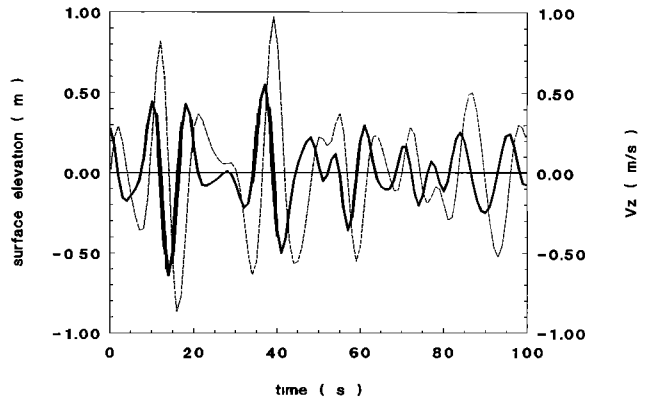

Figure 19. Predicted velocity V_z at free surface for the horizontal location of sensor 3 for case 2 (model: three waves, three sensors). Dashed curve, surface elevation; solid curve, velocity.

tures. Sometimes ship capsizings occur not because of extreme wave heights but because of sudden impacts by waves from different directions [*Kjeldsen*, 1990]. Furthermore, when wave directionality can be defined, the estimated forces on a structure can be 25–30% lower than when the waves are assumed to be unidirectional [*Dean*, 1977].

7. Conclusion and Further Work

The present method for a deterministic decomposition of short-crested ocean waves gives accurate predictions when applied to the available wave field measurements. It should be noted that the method is not limited to pressure head measurements and can be extended to allow for measurements of other wave characteristics, such as wave elevation and wave particle velocities. The novelty of our method is that there are no a priori assumptions regarding functional or statistical properties of free-wave components. The present method is, however, in its infant stage, and more research related to this method needs to be done before a final conclusion can be made. In the near future we plan to use the measurements of steeper waves generated in an multidirectional wave tank to validate this method and to implement the phase modulation approach in the method to model high-frequency wave components.

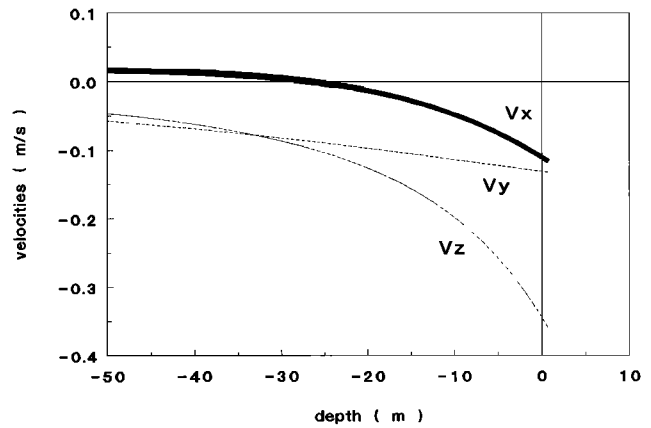

Figure 20. Particle velocities as functions of depth for the horizontal location of sensor 3 for case 2 (model: three waves, three sensors) at local time 40 s.

Appendix: Velocity Components

The solutions for horizontal velocity components V_x and V_y for two directional interacting waves are given by

$$V_x = \sum_{i=1}^{2} a_i \sigma_i e^{-k_i d} \cos(\beta_i) \cos(\theta_i)$$
$$+ a_1 a_2 e^{-|\mathbf{k}_1 - \mathbf{k}_2| d} B_0^- \omega_1 \omega_2 (\omega_1 - \omega_2)[\cos(\beta_1 - \beta_2) + 1]$$
$$\cdot (k_1 \cos\beta_1 - k_2 \cos\beta_2) \cos(\theta_1 - \theta_2)$$
$$+ a_1 a_2 e^{-|\mathbf{k}_1 + \mathbf{k}_2| d} B_0^+ \omega_1 \omega_2 (\omega_1 + \omega_2)[\cos(\beta_1 - \beta_2) - 1]$$
$$\cdot (k_1 \cos\beta_1 + k_2 \cos\beta_2) \cos(\theta_1 + \theta_2), \quad (28)$$

$$V_y = \sum_{i=1}^{2} a_i \sigma_i e^{-k_i d} \sin(\beta_i) \cos(\theta_i)$$
$$+ a_1 a_2 e^{-|\mathbf{k}_1 - \mathbf{k}_2| d} B_0^- \omega_1 \omega_2 (\omega_1 - \omega_2)[\cos(\beta_1 - \beta_2) + 1]$$
$$\cdot (k_1 \sin\beta_1 - k_2 \sin\beta_2) \cos(\theta_1 - \theta_2)$$
$$+ a_1 a_2 e^{-|\mathbf{k}_1 + \mathbf{k}_2| d} B_0^+ \omega_1 \omega_2 (\omega_1 + \omega_2)$$
$$\cdot [\cos(\beta_1 - \beta_2) - 1](k_1 \sin\beta_1 + k_2 \sin\beta_2)$$
$$\cdot \cos(\theta_1 + \theta_2). \quad (29)$$

Acknowledgments. This research was supported by the Offshore Technology Research Center, which is sponsored in part by National Science Foundation Engineering Research Centers Program grant CDR-8721512, the Texas Advance Technology Program, and the Joint Industry Program sponsored by Chevron, Exxon, Mobil, Shell, and Texaco. Without this support the research would not be possible. The Coastal Data Information Program, which made the field measurements available, is sponsored by the U.S. Army Engineers, the Coastal Engineering Research Center (CERC), and the California Department of Boating and Waterways. Their assistance is gratefully acknowledged. C. E. Long of CERC for sharing his expertise and C. Wang and D. J. Wisch of Texaco for providing the plots of the Harvest Platform are gratefully acknowledged.

References

Borgman, L. E., Irregular ocean waves: Kinematics and forces, in *The Sea*, vol. 9, *Ocean Engineering Science, Part A*, pp. 121–168, John Wiley, New York, 1990.

Brissette, F. P., and I. K. Tsanis, Estimation of wave directional spectra from pitch-roll buoy data, *J. Waterw. Port Coastal Ocean Eng.*, *120*(1), 93–115, 1994.

Capon, J., High-resolution frequency-wavenumber spectrum analysis, *Proc. IEEE*, *57*(8), 1408–1418, 1969.

Chase, J., L. J. Cote, W. Marks, E. Mehr, W. J. Pierson Jr., F. G. Rönne, G. Stephenson, R. C. Vetter, and R. G. Walden, The directional spectrum of a wind generated sea as determined from data obtained by the Stereo Wave Observation Project, Technical report, 267 pp., Dep. of Meteorol. and Oceanogr. and Eng. Stat. Group, Coll. of Eng., N. Y. Univ., New York, 1957.

Davis, E. D., and L. A. Regier, Methods for estimating directional wave spectra from multi-element arrays, *J. Mar. Res.*, *35*, 453–477, 1977.

Dean, R., Hybrid method of computing wave loading, paper presented at the 9th Offshore Technology Conference, Houston, Tex., 1977.

Donelan, M. A., J. Hamilton, and W. H. Hui, Directional spectra of wind-generated waves, *Philos. Trans. R. Soc. London, Ser. A*, *315*, 509–562, 1985.

Forristall, G. Z., Kinematics of directionally spread waves, in *Proceedings of the Conference on Directional Wave Spectra Application*, pp. 129–146, Am. Soc. of Civ. Eng., New York, 1981.

Forristall, G. Z., E. G. Ward, V. J. Cardone, and L. E. Borgmann, The directional spectra and kinematics of surface gravity waves in tropical storm Delia, *J. Phys. Oceanogr.*, *8*, 888–909, 1978.

Goda, Y., Simulation in examination of directional resolution, in *Proceedings of the Conference on Directional Wave Spectra Application*, pp. 387–407, Am. Soc. of Civ. Eng., New York, 1981.

Goda, Y., Directional wave spectrum and its application in coastal engineering, in *Proceedings of the International Conference on Hydrodynamics*, pp. 9–18, China Ocean Press, Beijing, 1994.

Hasselmann, K., On the non-linear energy transfer in a gravity-wave spectrum, 1, General theory, *J. Fluid Mech.*, *12*, 481–500, 1962.

Irani, G. B., B. L. Gotwols, and A. W. Bjerkaas, The 1978 ocean wave dynamics experiment, in *Wave Dynamics and Radio Probing of the Ocean Surface*, edited by O. M. Phillips and K. Hasselmann, pp. 165–179, Plenum, New York, 1986.

Kjeldsen, S. P., The practical value of directional ocean wave spectra, *Johns Hopkins APL Tech. Dig.*, *11*(3, 4), 381–387, 1990.

Long, R. B., Inverse modeling in ocean wave studies, in *Wave Dynamics and Radio Probing of the Ocean Surface*, edited by O. M. Phillips and K. Hasselmann, pp. 571–593, Plenum, New York, 1986.

Longuet-Higgins, M. S., Resonant interactions between two trains of gravity waves, *J. Fluid Mech.*, *12*, 321–332, 1962.

Masuda, A., Y. Kuo, and H. Mitsuyasu, On the dispersion relation of random gravity waves, 1, Theoretical framework, *J. Fluid Mech.*, *92*, 717–730, 1979.

Mitsuyasu, H., Y. Kuo, and A. Masuda, On the dispersion relation of random gravity waves, 2, An experiment, *J. Fluid Mech.*, *92*, 731–749, 1979.

Panicker, N. N., Review of techniques for directional wave spectra, in *International Symposium on Ocean Wave Measurement and Analysis*, vol. 1, pp. 669–688, Am. Soc. of Civ. Eng., New York, 1974.

Phillips, O. M., Surface wave physics—A survey, *Flow Res. Rep. 145*, 91 pp., Flow Res. Co. Div. of Flow Ind., Inc., Kent, Wash., 1979.

Press, W. H., S. A. Teukolsky, W. T. Vetterling, and B. P. Flannery, *Numerical Recipes in FORTRAN: The Art of Scientific Computing*, 2nd ed., 963 pp., Cambridge Univ. Press, New York, 1992.

Sand, S. E., Three-dimensional deterministic structure of ocean waves, *Ser. Pap. 24*, 177 pp., Inst. of Hydrodyn. and Hydraul. Eng., Tech. Univ. of Denmark, Horsholm, 1979.

Schäffer, H. A., and P. Hyllested, Analysis of multidirectional waves using deterministic decomposition, in *International Symposium: Waves—Physical and Numerical Modelling*, vol. 2, pp. 911–920, Dep. of Civ. Eng., Univ. of British Columbia, Vancouver, Canada, 1994.

Seymour, R. J., D. Castel, D. McGehee, J. Thomas, and W. O'Reilly, New technology in coastal wave monitoring, in *Ocean Wave Measurement and Analysis: Waves '93*, edited by O. T. Magoon and J. M. Hemsley, pp. 105–123, Am. Soc. of Civ. Eng., New York, 1993.

Spell, C. A., J. Zhang, and R. E. Randall, Hybrid wave model for unidirectional irregular waves, II, Comparison with laboratory measurements, *J. Appl. Ocean Res.*, *18*, 93–110, 1996.

Su, M. Y., and A. W. Green, Experimental studies of strong nonlinear interactions of deep-water gravity waves, in *Wave Dynamics and Radio Probing of the Ocean Surface*, edited by O. M. Phillips and K. Hasselmann, pp. 231–253, Plenum, New York, 1981.

van Heteren, J., H. Keijser, and B. Schaap, Comparison wave directional measuring systems, *Appl. Ocean Res.*, *10*, 128–143, 1988.

Zhang, J., K. Hong, and D. K. P. Yue, Effects of wavelength ratio on wave modeling, *J. Fluid Mech.*, *248*, 107–127, 1993.

Zhang, J., L. Chen, M. Ye, and R. E. Randall, Hybrid wave model for unidirectional irregular waves, I, Theory and numerical scheme, *J. Appl. Ocean Res.*, *18*, 77–92, 1996a.

Zhang, J., E. Meza Conde, and J. Yang, Wave elevation based on the pressure measurement at Latex Site 16, *COE Rep. 352*, Tex. A&M Univ., College Station, 1996b.

I. Prislin, Deep Oil Technology, Inc., 2300 Boswell Road, #210, Chula Vista, CA 91914.

R. J. Seymour, Offshore Technology Research Center, College Station, TX 77843-3400.

J. Zhang, Ocean Engineering Program, Department of Civil Engineering, Texas A&M University, College Station, TX 77843-3136. (e-mail: jun-zhang@tamu.edu)

(Received August 21, 1995; revised January 24, 1997; accepted February 11, 1997.)